

Theoretical analysis of electronic processes occurring during ultrafast demagnetization of cobalt, triggered by X-ray photons tuned to Co L₃ resonance.

Konrad J. Kapcia,^{1, 2, *} Victor Tkachenko,^{3, 4, 2, †} Flavio Capotondi,⁵ Alexander Lichtenstein,^{4, 6} Serguei Molodtsov,⁴ Leonard Mueller,⁷ Andre Philipp-Kobs,⁷ Przemysław Piekarz,³ and Beata Ziaja^{2, 3, ‡}

¹ Institute of Spintronics and Quantum Information, Faculty of Physics, Adam Mickiewicz University in Poznań, Uniwersytetu Poznańskiego 2, 61614 Poznań, Poland

² Center for Free-Electron Laser Science CFEL, Deutsches Elektronen-Synchrotron DESY, Notkestr. 85, 22607 Hamburg, Germany

³ Institute of Nuclear Physics, Polish Academy of Sciences, Radzikowskiego 152, 31-342 Kraków, Poland

⁴ European XFEL GmbH, Holzkoppel 4, 22869 Schenefeld, Germany

⁵ Elettra-Sincrotrone Trieste S.C.p.A, 34149 Trieste, Basovizza, Italy

⁶ University of Hamburg, Jungiusstr. 9, 20355 Hamburg, Germany

⁷ Deutsches Elektronen-Synchrotron DESY, Notkestr. 85, 22607 Hamburg, Germany

(Dated: July 14, 2022)

Magnetization dynamics triggered with ultrashort laser pulses has been attracting significant attention, with strong focus on the dynamics excited by VIS/NIR pulses. Only recently, strong magnetic response in solid materials induced by intense X-ray pulses from free-electron lasers (FELs) has been observed. The exact mechanisms that trigger the X-ray induced demagnetization are not yet fully understood. They are subject of on-going experimental and theoretical investigations. Here, we present a theoretical analysis of electronic processes occurring during demagnetization of Co multilayer system irradiated by X-ray pulses tuned to L₃-absorption edge of cobalt. We show that, similarly as in the case of X-ray induced demagnetization at M-edge of Co, electronic processes play a predominant role in the demagnetization until the pulse fluence does not exceed the structural damage threshold. The impact of electronic processes can reasonably well explain the available experimental data, without a need to introduce the mechanism of stimulated elastic forward scattering.

I. INTRODUCTION

Since its discovery [1], ultrafast demagnetization was studied mostly with lasers working in infrared regime [2–7]. X-ray induced ultrafast demagnetization has become a topic of intense studies after the commissioning of the new generation light sources, X-ray and XUV free electron lasers (FELs), see, e.g., [8–18]. The FELs produce ultrashort, intense, coherent, and wavelength-tunable X-ray pulses [19–22]. Such pulses give an opportunity to study demagnetization by using X-ray magnetic circular dichroism (XMCD) effect, with FEL photons of energy tuned to a dichroic absorption edge of a ferromagnetic element [3, 23–27]. The principle of XMCD is, in particular, explored in the resonant magnetic small angle X-ray scattering (mSAXS) measurements [8, 17, 28], where magnetic response of irradiated systems can be probed on femtosecond timescales. The experiments which employed resonant magnetic scattering with photons tuned to M-absorption edge of cobalt, acting either as a pump or a probe, are described in Refs. [8, 9, 11, 16, 17]. The experiments which employed resonant magnetic X-ray scattering at L-absorption edge of cobalt are described in [10, 13, 15]. Similar studies were also performed for nickel samples [29, 30].

The first theoretical explanation proposed for the observed loss of resonant magnetic scattering signal at M-edge of cobalt was proposed in [11]. The mechanism considered was the perturbation of the electronic state within the magnetic sample during the first few femtoseconds of exposure leading to the atomic levels shifts and to the resulting ultrafast quenching of the resonant magnetic scattering. However, the proposed mechanism was formulated in [11] rather as a hypothesis and not proven explicitly there. In the following X-ray studies at Co L-edge [12, 13, 15], the decreasing magnetic scattering signal was explained via stimulated elastic forward scattering in a simplified two-level atom model. However, this approach did not provide a full treatment of radiation damage caused by incoming X-ray photons. In particular, the two-level model approach could not account for the effect of electrons released during X-ray irradiation on electronic occupations within cobalt conduction band. Consequently, it did not accurately describe the magnetization dynamics triggered by photons tuned to M-edge of Co [17].

* e-mail: konrad.kapcia@amu.edu.pl; ORCID ID: [0000-0001-8842-1886](https://orcid.org/0000-0001-8842-1886)

† e-mail: victor.tkachenko@xfel.eu

‡ e-mail: ziaja@mail.desy.de

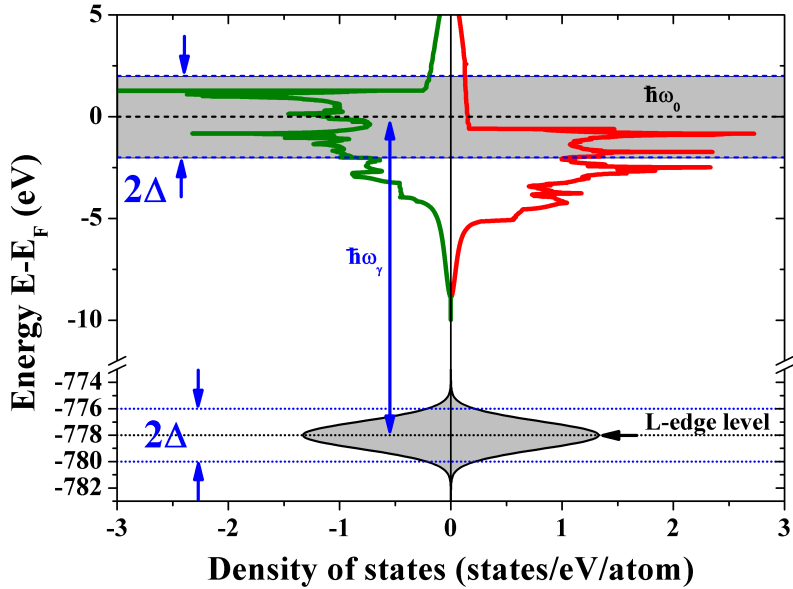


FIG. 1. Calculated density of states for equilibrium fcc cobalt, with schematic indication of the $2p$ band of cobalt, and of the probed region in its $3d$ band. The width of the $2p$ band is 2Δ . The density of states is shown for spin-up domain (red line) and for spin-down domain (green line).

In Ref. [18], we proposed a new modelling tool XSPIN, enabling a comprehensive nanoscopic description of electronic processes occurring in X-ray irradiated ferromagnetic materials. With this tool, we studied the response of Co/Pt multilayer system irradiated by an ultrafast XUV pulse tuned to M-edge of Co (photon energy ~ 60 eV), at the conditions corresponding to those of the experiment [17]. The XSPIN simulations showed that the magnetic scattering signal from cobalt decreased on femtosecond timescales due to electronic excitation, relaxation and transport processes, both in the cobalt and in the platinum layers. The signal decrease was stronger with the increasing fluence of incoming radiation, following the trend observed in the experimental data. Confirmation of the predominant role of electronic processes for X-ray induced demagnetization in the regime below the structural damage threshold, achieved with our theoretical study, was a step towards quantitative understanding of X-ray induced magnetic processes on femtosecond timescales.

In this work, we apply the XSPIN model to describe the results of the experiment on resonant X-ray scattering with photons tuned to L_3 -absorption edge of Co, performed at the Linac Coherent Light Source (LCLS) free-electron laser facility and presented in Ref. [13]. Although the electron kinetics following Co irradiation with X-ray photons of ~ 778 eV energy includes additional photoexcitation and relaxation channels such as inner-shell excitation and the resulting Auger processes, the electronic relaxation progresses in a similar way (through collisional processes) as after Co irradiation with 60 eV photons (M-edge case). Our purpose is to show that the collisional electronic relaxation is a universal mechanism that can explain ultrafast demagnetization of Co by X-ray pulses of low fluence, independently of X-ray photon energy.

In what follows, we will recall the details of the measurement performed in [13]. Afterwards, we will discuss the application of the XSPIN model to model demagnetization induced by X-ray photons tuned to Co L_3 edge. We will then present the model results compared to experimental data. Finally, our conclusions will be listed.

II. RESONANT X-RAY SCATTERING EXPERIMENT AT LCLS FACILITY

In the experiment performed by Wu et al. at the LCLS facility [13], the Co/Pd magnetic multilayer system was used. Its details are taken from Refs. [10, 13]. The multilayer system consisted of Ta(1.5nm)Pd(3nm) [Co(0.5nm)Pd(0.7nm)]₄₀ Pd(2nm) layers fixed on the Si_3N_4 membrane. A similar magnetic system was also used in [15]. For pumping and probing the system, the linearly polarized X-ray pulses of 778 ± 0.1 eV energy (monochromatized and tuned to the Co L_3 -edge absorption resonance) were applied. Their duration was 50 fs FWHM. The sample was covered by a radiation-opaque gold plate with a central hole of $1.45 \mu\text{m}$ diameter. XFEL pulses were focused onto the gold plate to a spot size of $10 \mu\text{m}$ FWHM. However, only a fraction of radiation arrived on the sample, i.e., the fraction passing through the central hole in the plate. We have checked that the average pulse fluence

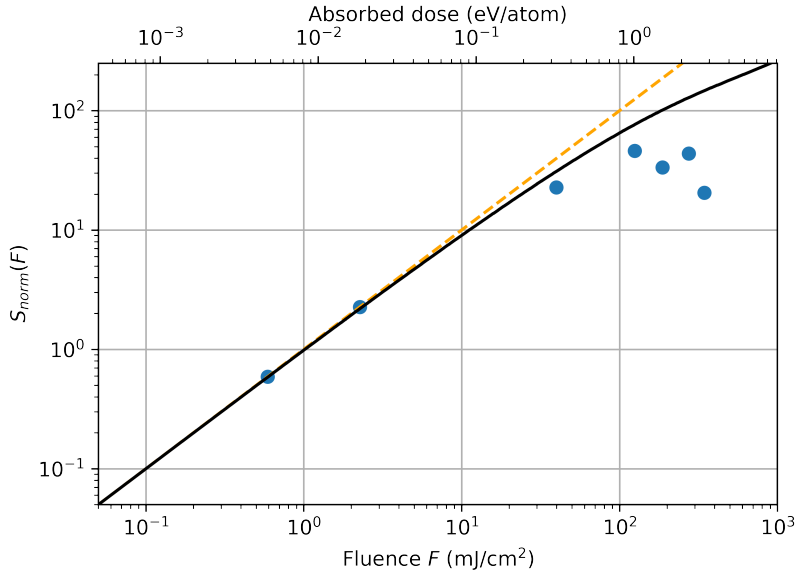


FIG. 2. Normalized magnetic scattering efficiency, $S_{norm}(F)$ as a function of the average absorbed dose, also converted into the effective pulse fluence (incoming on the uppermost Ta layer). Predictions including the demagnetization (black line), and predictions assuming no demagnetization, i.e., $M(t) = M(0)$ (orange dashed line) are shown for comparison. Experimental data are taken from Ref. [13]. The value of $\Delta = 2$ eV was used [23, 24].

in the aperture (i.e., the fraction of beam energy passing through the aperture, divided by the aperture size) was very similar to the average pulse fluence on the whole sample. The gold plate had also a few small holes outside the sample. The resulting X-ray diffraction patterns were recorded with a CCD detector. From the patterns, relative diffraction contrast of magnetic speckles was extracted for various values of the X-ray fluence. It was presented in Fig. 4(b) of Ref. [13]. This quantity reflected the decrease of the magnetic scattering strength with increasing pulse fluence. Our model predictions will be later compared to it.

III. XSPIN MODEL

In order to follow X-ray induced magnetization change in irradiated magnetic material the XSPIN code has been developed [18] as an extension of the hybrid code XTANT [31, 32]. XTANT is an established simulation tool, enabling to study electronic and structural transitions triggered in solids by X-rays. The XSPIN code includes all the predominant processes occurring in solids as a result of X-ray irradiation, i.e., inner-shell and conduction band photoabsorption, Auger decay and collisional (impact) ionization, as well as electron thermalization. In this work, we only consider electronic damage by X rays, assuming that the X-ray pulse fluence was too low to cause any structural damage resulting in atomic displacements. Although the dose absorbed per Co atom, needed to melt it thermally, seems rather low, $D_{melt} = 0.54$ eV/atom, this melting criterium is not directly applicable to the femtosecond regime studied, as much longer time (\sim few picoseconds) is needed to fully melt Co after the absorption of D_{melt} . Still, this dose gives a rough indication, at which value of the absorbed energy the processes leading to structural changes in Co can start to play a role.

The foundations of the XSPIN code have been described in [18]. There are two electronic subsystems – with spin-up and with spin-down electrons – considered in the model. Band structure for both subsystems is obtained from the density of states, $D_\sigma(\epsilon)$, calculated with the Vienna Ab initio Simulation Package (VASP) [33–36]. The energy levels in the low-energy electron fraction (here, containing electrons with energies less than 15 eV above the Fermi level) are determined from the total spin-polarized density of states $D_\sigma(\epsilon)$ calculated for fcc Co, see Fig. 1. The energy $E_{i,\sigma}$ of i -th level for spin- σ electrons is then calculated from the equation, $i = \int_{-\infty}^{E_{i,\sigma}} d\epsilon D_\sigma(\epsilon)$. It is assumed that all electrons from the low-energy-electron fraction, both within the spin-up and the spin-down subsystems, stay in a common local thermal equilibrium. Therefore, their occupations on individual energy levels follow the Fermi-Dirac distribution, depending on the actual *common* electronic temperature and the *common* chemical potential. By the assumption of the mutual instant thermalization between both electronic subsystems, we implicitly include spin-flip processes into our model.

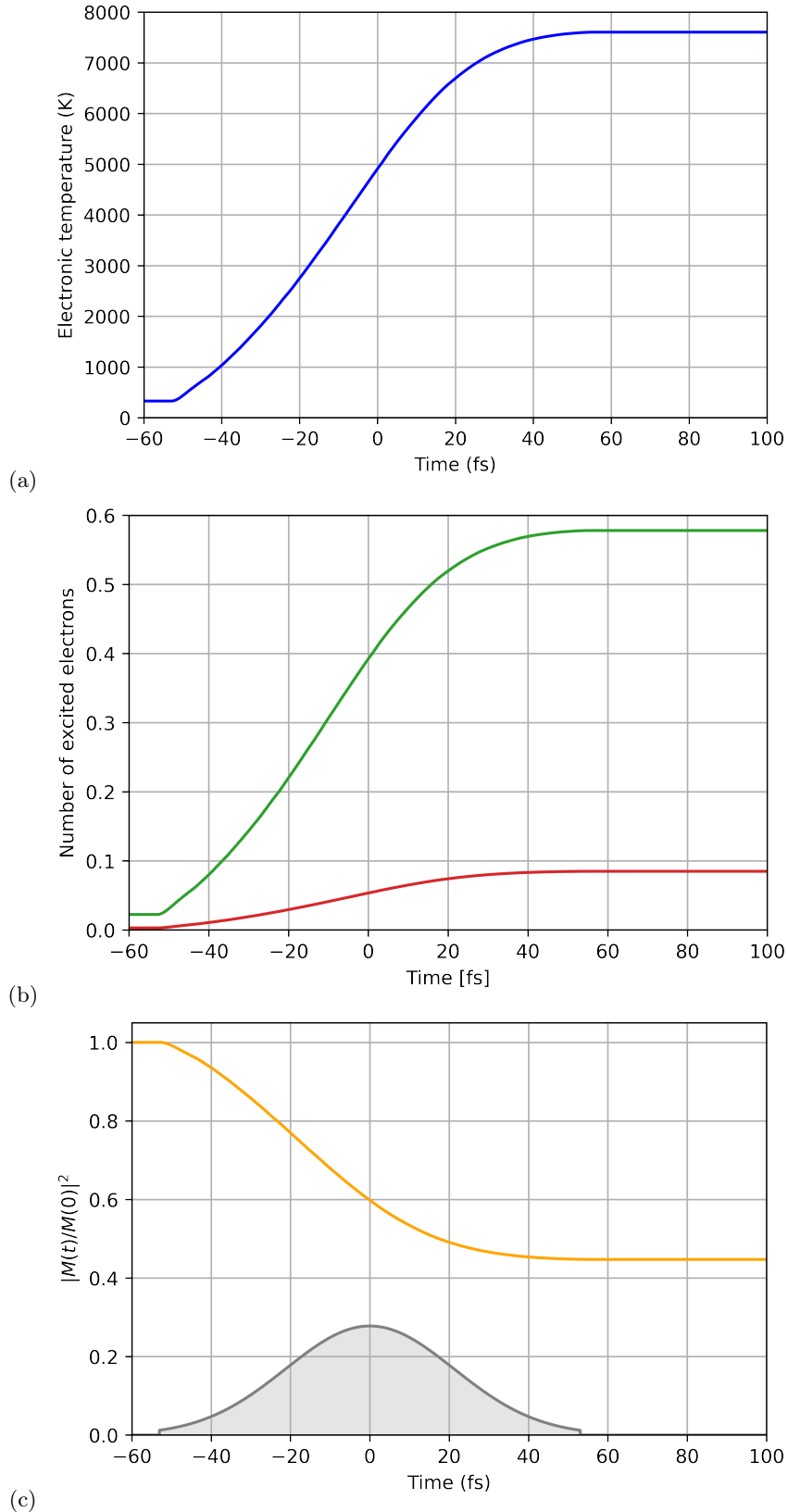


FIG. 3. Temporal evolution of: (a) electronic temperature; (b) number of excited electrons (per atom) in spin-up and spin-down domains. Red line denotes the spin-up (majority spin) electron fraction and green line denotes the spin-down (minority spin) electron fraction; (c) magnetization, with schematically plotted X-ray pulse shape. The average absorbed dose used for this simulation was 0.93 eV/atom. The value of $\Delta = 2.0$ eV was used for (c) [23, 24].

After an X-ray pulse starts to interact with a solid material, electrons from spin-up and spin-down subsystems are released due to the photoabsorption processes. The excitation probabilities take into account the actual electronic occupations in the respective bands. If the photon energy is sufficiently high to trigger an electronic excitation from a core shell, a spin-up or spin-down electron can be excited from the shell. After the photoabsorption, the energetic photoelectron joins the non-thermalized high-energy electron fraction (i.e., here with the energies above 15 eV above the Fermi level). During the sequence of the following impact ionization events, the electron continuously loses its energy and, depending on its spin, ultimately joins either the spin-up or the spin-down subsystem of the low-energy electron fraction. The high-energy electrons may collisionally excite secondary electrons, with the same or an opposite spin. The probability of such an excitation depends on the actual occupation of the spin-up and spin-down electron levels. Core holes relax via Auger decay. A band electron with the same spin fills the hole, while the Auger electron is chosen randomly, according to the actual distribution of spin-up and spin-down electrons.

The code XSPIN provides also the information on the strength of the resonant magnetic signal, scattered from the X-ray irradiated sample, i.e., the magnetic scattering efficiency $S(F)$. It is equal to the convolution of the incoming beam intensity and the actual magnetization of the sample [16, 18, 37]:

$$S(F) = \int_{-\infty}^{+\infty} dt I(t) M^2(t), \quad (1)$$

where the time-dependent magnetization $M(t)$ reflects the disparity between electronic populations at the resonant states in spin-up and spin-down electronic subsystems:

$$M(t) = \sum_{\hbar\omega_0 - \Delta}^{\hbar\omega_0 + \Delta} \left[N_{\uparrow}^{\text{hole}}(E_{i,\uparrow}) - N_{\downarrow}^{\text{hole}}(E_{i,\downarrow}) \right], \quad (2)$$

with $N_{\sigma}^{\text{hole}}(E_{i,\sigma})$ denoting the number of empty states at the $E_{i,\sigma}$ level. The XSPIN code calculates transient changes of $N_{\sigma}^{\text{hole}}(E_{i,\sigma})$ in response to a specific X-ray pulse for the probed energy levels within the Co 2p band, i.e., within the interval $\pm\Delta$ around the probed level $\hbar\omega_0$ (Fig. 1). To explain it in more detail, the incoming X-ray photons of energy, $\hbar\omega_{\gamma}$, excite electrons from the 2p levels to the 3d band (conduction band). The region in the 3d band, to which electrons are excited, then extends from $\hbar\omega_0 - \Delta$ to $\hbar\omega_0 + \Delta$, where $\hbar\omega_0$ is the difference between the photon energy and the position of L-edge: $\hbar\omega_0 = \hbar\omega_{\gamma} - E_{\text{edge}}$, with $E_{\text{edge}} = 778$ eV for L-edge of Co. Here, 2Δ is the 2p band width, which determines the number of states probed in the 3d band.

IV. RESULTS

For the photon energy tuned slightly above L-edge of Co ($E_{\gamma} = 778.2$ eV), the attenuation length of X-rays in Co is 73.1 nm, in Pd 73.4 nm, and in Ta 100 nm. If we compare these numbers with the overall size of the multilayer system, used in the experiment [13], we can conclude that the X-ray energy is absorbed to a large extent homogeneously in the sample. In addition, energetic electrons emitted as a result of photoabsorption spread out on large distances within the sample (the electron ranges are 7.0 nm for Co and 7.5 nm for Pd). This additionally reinforces the homogeneity of the energy distribution in the sample. Therefore, we can estimate and use the same average effective absorbed dose for each of the Co layers. Assuming the homogeneous distribution of secondary electrons in the whole sample after the electron transport, the effective dose corresponds to the average dose absorbed per Co atom, needed to create the estimated average number of electrons in a Co layer. This finding is in contrast to the XSPIN calculations in [18], where the energy absorption was strongly inhomogeneous in the multilayer system, even after the interlayer electron transport was included.

XSPIN simulations were performed for supercells with periodic boundary conditions consisting of 512 atoms of Co. This number of atoms ensured stability and convergence of the calculations. The atomic positions corresponded to the atomic positions in the equilibrium fcc cobalt. Atoms were kept frozen, i.e., no X-ray induced structural modifications in Co or Pt were taken into account. With the XSPIN predictions obtained for time-dependent magnetization $M(t)$ at various values of the absorbed dose, we calculated the magnetic scattering signal $S(F)$. Figure 2 presents the results for the normalized magnetic scattering signal at $\Delta = 2.0$ eV. This Δ value corresponds to the half of the FWHM of the Co L-edge resonance peak [23, 24, 38, 39]. Similarly as in [18], the normalized signal is defined as $S_{\text{norm}}(F) = S(F) \cdot F_0 / S(F_0)$, where $F_0 = 0.01$ mJ/cm². One can see initially a linear increase of $S_{\text{norm}}(F)$ with the pulse fluence. At the doses above 0.24 eV/atom (fluences higher than 30 mJ/cm²), the curve starts to bend down and becomes non-linear, similarly as observed in [18]. The results are compared with the experimental data from [13] after converting the dose into pulse fluence arriving on Ta upper layer. There is a disagreement between the data and

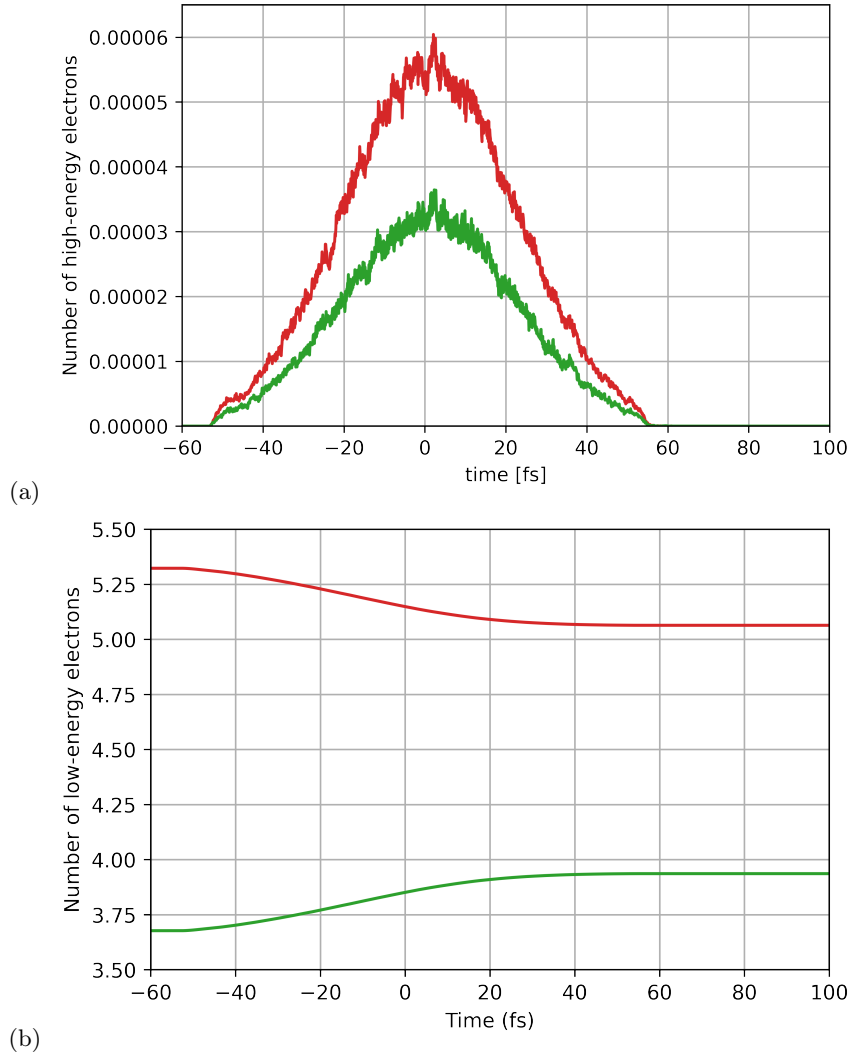


FIG. 4. (a) Number of high energy electrons, and (b) number of low energy electrons (both per atom) as a function of time. Red line denotes the spin-up (majority spin) electron fraction and green line denotes the spin-down (minority spin) electron fraction. The results were obtained for the average absorbed dose of 0.93 eV/atom.

theory predictions at higher fluence values. This is the regime above the structural damage threshold (0.54 eV/atom) where the frozen-atom approximation may be not fully applicable, even at the short timescales considered.

In order to understand the processes behind the change of magnetic scattering signal observed, we analyzed the simulation results in detail. Figure 3 presents temporal evolution of electron temperature, transient number of excited electrons (with energies above the Fermi level) per atom, and a typical shape of demagnetization curve $M^2(t)$ obtained for $\Delta = 2.0$ eV, and normalized to its initial value. The temporal Gaussian profile of the X-ray pulse, with the duration of 50 fs FWHM is also shown. The absorbed dose was in this case 0.93 eV/atom. For this dose, one observes a 55 % decrease of $M^2(t)$, when compared with its initial value at $t = 0$ fs. The decrease of the magnetization is related to the increase of the number of excited electrons (i.e., the electrons with the energy above the Fermi level; Fig. 3b) and the increase of electronic temperature (Fig. 3a). It is clearly seen (Fig. 3b) that more spin-down (minority spin) electrons are excited than spin-up (majority spin) electrons. This is due to the 'asymmetry' between spin-up and spin-down bands (Fig. 1), i.e., the different density of states for each spin orientation and the different energy level structure in each spin domain. For the spin-down domain, more energy levels are available above the Fermi level, and consequently, more electrons get excited there. We have checked that although the number of spin-down and spin-up electrons is different, the energy absorbed in each of the electronic subsystems is comparable, as expected.

In Figure 4, we present time evolution of the total number of high-energy electrons (with energies above 15 eV) and low energy electrons (with energies below 15 eV) normalized per atom. The number of high-energy electrons is relatively small and its evolution follows the intensity profile of the X-ray pulse. The transient number of high-

energy spin-up electrons is larger than the number of high-energy spin-down electrons (Fig. 4a). Still, due to the above mentioned 'asymmetry' between spin-up and spin-down bands, more electrons get excited to the low-energy spin-down domain during the collisional relaxation of high-energy electrons (Fig. 4b). As the result, the total number of spin-up electrons in the low-energy domain decreases and the total number of spin-down electrons respectively increases. Ultimately, this drives the change of Co magnetization, depicted in Fig. 3c.

V. CONCLUSIONS

In summary, we analyzed the role of electronic processes for ultrafast demagnetization in cobalt, triggered by X-ray photons tuned to L-edge of Co. The simulations performed with our computational tool XSPIN (which was already successful in describing magnetization dynamics triggered by photons tuned to M-edge of Co [18]), when compared to the L-edge data recorded a few years ago at the LCLS facility [13], proved a strong effect of electronic processes also for this case. More experimental data are needed for model validation in the 'destructive' fluence regime (i.e., for absorbed doses > 0.54 eV/atom). However, already now it is clear that the X-ray driven ultrafast rearrangement of electronic occupations within the magnetically sensitive bands of cobalt strongly impacts its magnetic properties. This observation opens a pathway towards quantitative control and manipulation of X-ray induced magnetic processes on femto- to picosecond timescales.

ACKNOWLEDGMENTS

B. Z. thanks A. Scherz and S. Parchenko for helpful discussions. K. J. K. thanks the Polish National Agency for Academic Exchange for funding in the frame of the Bekker programme (PPN/BEK/2020/1/00184). K. J. K. is also grateful for the funding from the scholarships of the Minister of Science and Higher Education (Poland) for outstanding young scientists (2019 edition, No. 821/STYP/14/2019). V. T. and B. Z. acknowledge the funding received from the Collaboration Grant of the European XFEL and the Institute of Nuclear Physics, Polish Academy of Sciences.

[1] E. Beaurepaire, J.-C. Merle, A. Daunois, and J.-Y. Bigot, Ultrafast spin dynamics in ferromagnetic nickel, *Phys. Rev. Lett.* **76**, 4250 (1996).

[2] B. Koopmans, G. Malinowski, F. D. Longa, D. Steiauf, M. Fahnle, T. Roth, M. Cinchetti, and M. Aeschlimann, Explaining the paradoxical diversity of ultrafast laser-induced demagnetization, *Nat. Mat.* **9**, 259 (2010).

[3] A. Kirilyuk, A. V. Kimel, and T. Rasing, Ultrafast optical manipulation of magnetic order, *Rev. Mod. Phys.* **82**, 2731 (2010).

[4] M. Battiato, K. Carva, and P. M. Oppeneer, Superdiffusive Spin Transport as a Mechanism of Ultrafast Demagnetization, *Phys. Rev. Lett.* **105**, 027203 (2010).

[5] K. Carva, M. Battiato, and P. M. Oppeneer, Ab Initio Investigation of the Elliott-Yafet Electron-Phonon Mechanism in Laser-Induced Ultrafast Demagnetization, *Phys. Rev. Lett.* **107**, 207201 (2011).

[6] M. Battiato, K. Carva, and P. M. Oppeneer, Theory of laser-induced ultrafast superdiffusive spin transport in layered heterostructures, *Phys. Rev. B* **86**, 024404 (2012).

[7] D. Sander, S. O. Valenzuela, D. Makarov, C. H. Marrows, E. E. Fullerton, P. Fischer, J. McCord, P. Vavassori, S. Mangin, P. Pirro, B. Hillebrands, A. D. Kent, T. Jungwirth, O. Gutfleisch, C. G. Kim, and A. Berger, The 2017 Magnetism Roadmap, *J. Phys. D* **50**, 363001 (2017).

[8] C. Gutt, S. Streit-Nierobisch, L.-M. Stadler, B. Pfau, C. M. Günther, R. Könnecke, R. Frömter, A. Kobs, D. Stickler, H. P. Oepen, R. R. Fäustlin, R. Treusch, J. Feldhaus, E. Weckert, I. A. Vartanyants, M. Grunze, A. Rosenhahn, T. Wilheim, S. Eisebitt, and G. Grübel, Single-pulse resonant magnetic scattering using a soft X-ray free-electron laser, *Phys. Rev. B* **81**, 100401(R)s (2010).

[9] B. Pfau, S. Schaffert, L. Müller, C. Gutt, A. Al-Shemmary, F. Büttner, R. Delaunay, S. Düsterer, S. Flewett, R. Frömter, J. Geilhufe, E. Guehrs, C. M. Günther, R. Hawaldar, M. Hille, N. Jaouen, A. Kobs, K. Li, J. Mohanty, H. Redlin, W. F. Schlotter, D. Stickler, R. Treusch, B. Vodungbo, M. Kläui, H. P. Oepen, J. Lüning, G. Grübel, and S. Eisebitt, Ultrafast optical demagnetization manipulates nanoscale spin structure in domain walls, *Nat. Commun.* **3**, 1100 (2012).

[10] T. Wang, D. Zhu, B. Wu, C. Graves, S. Schaffert, T. Rander, L. Müller, B. Vodungbo, C. Baumier, D. P. Bernstein, B. Bräuer, V. Cros, S. de Jong, R. Delaunay, A. Fognini, R. Kukreja, S. Lee, V. López-Flores, J. Mohanty, B. Pfau, H. Popescu, M. Sacchi, A. B. Sardinha, F. Sirotti, P. Zeitoun, M. Messerschmidt, J. J. Turner, W. F. Schlotter, O. Hellwig, R. Mattana, N. Jaouen, F. Fortuna, Y. Acremann, C. Gutt, H. A. Dürr, E. Beaurepaire, C. Boeglin, S. Eisebitt, G. Grübel, J. Lüning, J. Stöhr, and A. O. Scherz, Femtosecond single-shot imaging of nanoscale ferromagnetic order in Co/Pd multilayers using resonant X-ray holography, *Phys. Rev. Lett.* **108**, 267403 (2012).

[11] L. Müller, C. Gutt, B. Pfau, S. Schaffert, J. Geilhufe, F. Büttner, J. Mohanty, S. Flewett, R. Treusch, S. Düsterer, H. Redlin, A. Al-Shemmary, M. Hille, A. Kobs, R. Frömler, H. P. Oepen, B. Ziaja, N. Medvedev, S.-K. Son, R. Thiele, R. Santra, B. Vodungbo, J. Lüning, S. Eisebitt, and G. Grübel, Breakdown of the X-ray resonant magnetic scattering signal during intense pulses of extreme ultraviolet free-electron-laser radiation, *Phys. Rev. Lett.* **110**, 234801 (2013).

[12] J. Stöhr and A. Scherz, Creation of X-Ray Transparency of Matter by Stimulated Elastic Forward Scattering, *Phys. Rev. Lett.* **115**, 107402 (2015).

[13] B. Wu, T. Wang, C. E. Graves, D. Zhu, W. F. Schlotter, J. J. Turner, O. Hellwig, Z. Chen, H. A. Dürr, A. Scherz, and J. Stöhr, Elimination of X-ray diffraction through stimulated x-ray transmission, *Phys. Rev. Lett.* **117**, 027401 (2016).

[14] F. Willems, C. von Korff Schmising, D. Weder, C. M. Günther, M. Schneider, B. Pfau, S. Meise, E. Guehrs, J. Geilhufe, A. E. D. Merhe, E. Jal, B. Vodungbo, J. Lüning, B. Mahieu, F. Capotondi, E. Pedersoli, D. Gauthier, M. Manfredda, and S. Eisebitt, Multi-color imaging of magnetic Co/Pt heterostructures, *Structural Dynamics* **4**, 014301 (2017).

[15] Z. Chen, D. J. Higley, M. Beye, M. Hantschmann, V. Mehta, O. Hellwig, A. Mitra, S. Bonetti, M. Bucher, S. Carron, T. Chase, E. Jal, R. Kukreja, T. Liu, A. H. Reid, G. L. Dakovski, A. Föhlisch, W. F. Schlotter, H. A. Dürr, and J. Stöhr, Ultrafast self-induced X-Ray transparency and loss of magnetic diffraction, *Phys. Rev. Lett.* **121**, 137403 (2018).

[16] M. Schneider, B. Pfau, C. M. Günther, C. von Korff Schmising, D. Weder, J. Geilhufe, J. Perron, F. Capotondi, E. Pedersoli, M. Manfredda, M. Hennecke, B. Vodungbo, J. Lüning, and S. Eisebitt, Ultrafast demagnetization dominates fluence dependence of magnetic scattering at Co M edges, *Phys. Rev. Lett.* **125**, 127201 (2020).

[17] A. Philippi-Kobs, L. Müller, M. H. Berntsen, W. Roseker, M. Riepp, K. Bagschik, J. Wagner, R. Frömler, M. Danailov, F. Capotondi, E. Pedersoli, M. Manfredda, M. Kiskinova, M. Stransky, V. Lipp, A. Scherz, B. Ziaja, H. P. Oepen, and G. Grübel, Ultrafast demagnetization excited by extreme ultraviolet light from a free-electron laser, <https://www.researchsquare.com/article/rs-955056/v1> (2021).

[18] K. J. Kapcia, V. Tkachenko, F. Capotondi, A. Lichtenstein, S. Molodtsov, L. Mueller, A. Philippi-Kobs, P. Piekarz, and B. Ziaja, Role of electronic excitation, relaxation and transport processes for X-ray induced ultrafast demagnetization within magnetic multilayer systems, [arXiv:2202.13845](https://arxiv.org/abs/2202.13845) (2022).

[19] W. Ackermann, G. Asova, V. Ayvazyan, A. Azima, N. Baboi, J. Bähr, V. Balandin, B. Beutner, A. Brandt, A. Bolzmann, R. Brinkmann, O. I. Brovko, M. Castellano, P. Castro, L. Catani, E. Chiadroni, S. Choroba, A. Cianchi, J. T. Costello, D. Cubaynes, J. Dardis, W. Decking, H. Delsim-Hashemi, A. Delserieys, G. Di Pirro, M. Dohlus, S. Düsterer, A. Eckhardt, H. T. Edwards, B. Faatz, J. Feldhaus, K. Flöttmann, J. Frisch, L. Fröhlich, T. Garvey, U. Gensch, Ch. Gerth, M. Görler, N. Golubeva, H.-J. Grabosch, M. Grecki, O. Grimm, K. Hacker, U. Hahn, J. H. Han, K. Honkavaara, T. Hott, M. Hüning, Y. Ivanisenko, E. Jaeschke, W. Jalmuzna, T. Jezynski, R. Kammering, V. Katalev, K. Kavanagh, E. T. Kennedy, S. Khodyachykh, K. Klose, V. Kocharyan, M. Körfer, M. Kollewe, W. Koprek, S. Korepanov, D. Kostin, M. Krassilnikov, G. Kube, M. Kuhlmann, C. L. S. Lewis, L. Lilje, T. Limberg, D. Lipka, F. Löhl, H. Luna, M. Luong, M. Martins, M. Meyer, P. Michelato, V. Miltchev, W. D. Möller, L. Monaco, W. F. O. Müller, O. Napieralski, O. Napoly, P. Nicolosi, D. Nölle, T. Nuñez, A. Oppelt, C. Pagani, R. Paparella, N. Pchalek, J. Pedregosa-Gutierrez, B. Petersen, B. Petrosyan, G. Petrosyan, L. Petrosyan, J. Pflüger, E. Plönjes, L. Poletto, K. Pozniak, E. Prat, D. Proch, P. Pucyk, P. Radcliffe, H. Redlin, K. Rehlich, M. Richter, M. Roehrs, J. Roensch, R. Romaniuk, M. Ross, J. Rossbach, V. Rybníkov, M. Sachwitz, E. L. Saldin, W. Sandner, H. Schlarb, B. Schmidt, M. Schmitz, P. Schmüser, J. R. Schneider, E. A. Schneidmiller, S. Schnepp, S. Schreiber, M. Seidel, D. Sertore, A. V. Shabunov, C. Simon, S. Simrock, E. Sombrowski, A. A. Sorokin, P. Spankebel, R. Spesvtsev, L. Staykov, B. Steffen, F. Stephan, F. Stulle, H. Thom, K. Tiedtke, M. Tischer, S. Toleikis, R. Treusch, D. Trines, I. Tsakov, E. Vogel, T. Weiland, H. Weise, M. Wellhöfer, M. Wendt, I. Will, A. Winter, K. Wittenburg, W. Wurth, P. Yeates, M. V. Yurkov, I. Zagorodnov, and K. Zapfe, Operation of a free-electron laser from the extreme ultraviolet to the water window, *Nat. Photonics* **1**, 336 (2007).

[20] P. Emma, R. Akre, J. Arthur, R. Bionta, C. Bostedt, J. Bozek, A. Brachmann, P. Bucksbaum, R. Coffee, F.-J. Decker, Y. Ding, D. Dowell, S. Edstrom, A. Fisher, J. Frisch, S. Gilevich, J. Hastings, G. Hays, P. Hering, Z. Huang, R. Iverson, H. Loos, M. Messerschmidt, A. Miahnahri, S. Moeller, H.-D. Nuhn, G. Pile, D. Ratner, J. Rzepiela, D. Schultz, T. Smith, P. Stefan, H. Tompkins, J. Turner, J. Welch, W. White, J. Wu, G. Yocky, and J. Galayda, First lasing and operation of an ångstrom-wavelength free-electron laser, *Nat. Photonics* **4**, 641 (2010).

[21] D. Pile, First light from SACLA, *Nat. Photonics* **5**, 456 (2011).

[22] E. Allaria, R. Appio, L. Badano, W. A. Barletta, S. Bassanese, S. G. Biedron, A. Borga, E. Busetto, D. Castronovo, P. Cinquegrana, S. Cleva, D. Cocco, M. Cornacchia, P. Craievich, I. Cudin, G. D'Auria, M. Dal Forno, M. B. Danailov, R. De Monte, G. De Ninno, P. Delgiusto, A. Demidovich, S. D. Mitri, B. Diviacco, A. Fabris, R. Fabris, W. Fawley, M. Ferianis, E. Ferrari, S. Ferry, L. Frehlich, P. Furlan, G. Gaio, F. Gelmetti, L. Giannessi, M. Giannini, R. Gobessi, R. Ivanov, E. Karantzoulis, M. Lonza, A. Lutman, B. Mahieu, M. Milloch, S. V. Milton, M. Musardo, I. Nikolov, S. Noe, F. Parmigiani, G. Penco, M. Petronio, L. Pivetta, M. Predonzani, F. Rossi, L. Rumiz, A. Salom, C. Scafuri, C. Serpico, P. Sigalotti, S. Spampinati, C. Spezzani, M. Svandrlík, C. Svetina, S. Tazzari, M. Trovo, R. Umer, A. Vascotto, M. Veronese, R. Visintini, M. Zaccaria, D. Zangrandino, and M. Zangrandino, Highly coherent and stable pulses from the FERMI seeded free-electron laser in the extreme ultraviolet, *Nat. Photonics* **6**, 699 (2012).

[23] C. T. Chen, Y. U. Idzerda, H.-J. Lin, N. V. Smith, G. Meigs, E. Chaban, G. H. Ho, E. Pellegrin, and F. Sette, Experimental confirmation of the x-ray magnetic circular dichroism sum rules for iron and cobalt, *Phys. Rev. Lett.* **75**, 152 (1995).

[24] R. Nakajima, J. Stöhr, and Y. U. Idzerda, Electron-yield saturation effects in l-edge x-ray magnetic circular dichroism spectra of Fe, Co, and Ni, *Phys. Rev. B* **59**, 6421 (1999).

[25] J. P. Hill and D. McMorrow, X-ray resonant exchange scattering: Polarization dependence and correlation functions, *Acta Cryst. A* **52**, 236 (1996).

[26] J. P. Hannon, G. T. Trammell, M. Blume, and D. Gibbs, X-ray resonance exchange scattering, *Phys. Rev. Lett.* **61**, 1245 (1988).

[27] F. Capotondi, E. P. N. M. R. H. Menk, G. Passos, L. Raimondi, C. Svetina, G. Sandrin, M. Zangrandi, M. Kiskinova, S. Bajt, M. Barthelmess, H. Fleckenstein, H. N. Chapman, J. Schulz, J. Bach, R. Frömter, S. Schleitzer, L. Müller, C. Gutt, and G. Grübel, Invited Article: Coherent imaging using seeded free-electron laser pulses with variable polarization: First results and research opportunities, *Rev. Sci. Instrum.* **84**, 051301 (2013).

[28] M. Riepp, K. Bagschik, F. Capotondi, R. Frömter, T. Golz, G. Grübel, M. Kiskinova, L. Müller, D. Naumenko, H. Oepen, E. Pedersoli, A. Philipp-Kobs, W. Roseker, R. Rysov, N. Stojanovic, and M. Walther, Ultrafast Magnetisation Dynamics at the Low-Fluence Limit Supported by External Magnetic Fields, in *39th Free Electron Laser Conference (FEL'19), Hamburg, Germany, 26-30 August 2019* (JACOW Publishing, Geneva, Switzerland, 2019) pp. 574–577.

[29] C. Stamm, T. Kachel, N. Pontius, R. Mitzner, T. Quast, K. Holldack, S. Khan, C. Lupulescu, E. F. Aziz, M. Wietstruk, H. A. Dürr, and W. Eberhardt, Femtosecond modification of electron localization and transfer of angular momentum in nickel, *Nat. Mat.* **6**, 740 (2007).

[30] M. Hennes, B. Rösner, V. Chardonnet, G. S. Chiuzbaian, R. Delaunay, F. Döring, V. A. Guzenko, M. Hehn, R. Jarrier, A. Kleibert, M. Lebugle, J. Lüning, G. Malinowski, A. Merhe, D. Naumenko, I. P. Nikolov, I. Lopez-Quintas, E. Pedersoli, T. Savchenko, B. Watts, M. Zangrandi, C. David, F. Capotondi, B. Vodungbo, and E. Jal, Time-resolved XUV absorption spectroscopy and magnetic circular dichroism at the Ni M_{2,3}-edges, *Applied Sciences* **11**, 325 (2021).

[31] N. Medvedev, H. O. Jeschke, and B. Ziaja, Nonthermal phase transitions in semiconductors induced by a femtosecond extreme ultraviolet laser pulse, *New J. Phys.* **15**, 015016 (2013).

[32] N. Medvedev, V. Tkachenko, V. Lipp, Z. Li, and B. Ziaja, Various damage mechanisms in carbon and silicon materials under femtosecond X-ray irradiation, *4open* **1**, 3 (2018).

[33] The Vienna Ab initio Simulation Package: Atomic scale materials modelling from first principles, <https://www.vasp.at>.

[34] G. Kresse and J. Hafner, Ab initio molecular-dynamics simulation of the liquid-metal–amorphous–semiconductor transition in germanium, *Phys. Rev. B* **49**, 14251 (1994).

[35] G. Kresse and J. Furthmüller, Efficient iterative schemes for ab initio total-energy calculations using a plane-wave basis set, *Phys. Rev. B* **54**, 11169 (1996).

[36] G. Kresse and D. Joubert, From ultrasoft pseudopotentials to the projector augmented-wave method, *Phys. Rev. B* **59**, 1758 (1999).

[37] J. Stöhr and H. C. Siegmann, Magnetism: From fundamentals to nanoscale dynamics, *Springer Series in Solid-State Sciences* (Springer Berlin, Heidelberg) (2006).

[38] A. M. Hibberd, H. Q. Doan, E. N. Glass, F. M. F. de Groot, C. L. Hill, and T. Cuk, Co polyoxometalates and a Co₃O₄ thin film investigated by L-edge X-ray absorption spectroscopy, *The Journal of Physical Chemistry C* **119**, 4173 (2015).

[39] M. Guo, X. Liu, and R. He, Restricted active space simulations of the metal L-edge X-ray absorption spectra and resonant inelastic X-ray scattering: revisiting [CoII/III(bpy)3]2+/3+ complexes, *Inorg. Chem. Front.* **7**, 1927 (2020).